Journal of Power Sources 233 (2013) 259–268

Contents lists available at SciVerse ScienceDirect

Journal of Power Sources

journal homepage: www.elsevier.com/locate/jpowsour

Cross-linked anion exchange membranes for alkaline fuel cells synthesized using a solvent free strategy

Xiaocheng Lin [a], Yanbo Liu [a], Simon D. Poynton [b], Ai Lien Ong [b], John R. Varcoe [b], Liang Wu [a], Yan Li [a], Xuhao Liang [a], Qiuhua Li [a], Tongwen Xu [a,*]

[a] CAS Key Laboratory of Soft Matter Chemistry, Laboratory of Functional Membranes, School of Chemistry and Materials Science, University of Science and Technology of China, Hefei, Anhui 230026, PR China
[b] Department of Chemistry, Faculty of Engineering and Physical Sciences, The University of Surrey, Guildford GU2 7XH, United Kingdom

HIGHLIGHTS

- Cross-linked AEMs were synthesized using a solvent free strategy.
- Such method is of environment and economic benefits.
- TEPA as a cross-linker greatly improves the membrane properties.
- AEMs herein are suitable for the AEMFCs application.

ARTICLE INFO

Article history:
Received 25 September 2012
Received in revised form
18 December 2012
Accepted 11 January 2013
Available online 17 January 2013

Keywords:
Cardo polyetherketone
Anion exchange membrane
Fuel cells
Solvent free
In situ bulk polymerization

ABSTRACT

This article describes the preparation of cross-linked anion exchange membranes (AEMs) using a solvent free strategy. A novel casting solution is formed by dissolving cardo polyetherketone (PEK-C) as an essential polymer intensifier in a mixture of vinylbenzyl chloride (VBC) and divinylbenzene (DVB) monomers without any organic solvent. Tetraethylenepentamine (TEPA) is added to act as a cross-linker between VBC and PKE-C. Polymerization and quaternization are successively implemented to obtain the cross-linked AEMs, whose properties are found to compare well to many referenced AEMs. Apart from improving the compatibility of PEK-C with poly(VBC-co-DVB), TEPA also effectively enhances the charge density, ionic conductivity and alkaline stabilities of the resulting AEMs, whilst simultaneously inhibiting the swelling ratio. The optimal membrane shows an ionic conductivity of 76 mS cm^{-1} at 70 °C and 100% relative humidity and can remain stable after immersing in 2 mol dm^{-3} KOH solution for 168 h. A power density of 6 mW cm^{-2} is achieved in a H_2/O_2 fuel cell test at 50 °C with an optimal AEM but a non-optimized membrane electrode fabrication process. Generally, the novel method herein highlights an environmentally friendly and economically attractive method for the preparation of AEMs used in alkaline fuel cells.

1. Introduction

Alkaline polymer electrolyte fuel cells (APEFCs) are attracting considerable interest due to several potential advantages over their acidic counterpart proton-exchange membrane fuel cells (PEMFCs) [1–4]. For example, the oxygen reduction kinetics is improved and there is better fuel oxidation kinetics in the high pH regime. Such improvement can theoretically lead to the higher electrical efficiencies as well as permit the use of a lower quantities of precious-metal-electro-catalysts or even their replacement with non-precious alternatives such as silver, nickel or manganese oxides [5–7] (greatly reducing the cost of the device). An anion exchange membrane (AEM) is a crucial component of APEFCs as it acts as a barrier between the fuel and oxidant streams while simultaneously transports ions from the cathode to the anode; this component therefore requires considerable development. Unfortunately, there is still no readily available benchmark AEM for APEFCs and this has resulted in the recent intensive worldwide efforts into the development of AEMs with performance characteristics suitable for use in APEFCs.

To date, the most commonly studied AEMs are based on quaternary ammonium (QA) functional group chemistry. They are generally prepared by the chloromethylation of the pristine polymers, such as poly (phthalazinon ether sulfone ketone) (PPESK) [8],

* Corresponding author.
E-mail address: twxu@ustc.edu.cn (T. Xu).

0378-7753/$ – see front matter © 2013 Elsevier B.V. All rights reserved.
http://dx.doi.org/10.1016/j.jpowsour.2013.01.059

polysulfone (PS) [9] and poly (ether ketone) (PEK) [10], followed by quaternization with trimethylamine (TMA). Another approach for the preparation of AEMs is direct polymerization of monomers that contain a moiety that is, or can be transformed into, tetraalkylammonium groups [4]. Chu et al. reported the copolymerization of methyl methacrylate, vinylbenzyl chloride and divinylbenzene cross-linker followed by quaternization [11]. Clark et al. recently reported the synthesis of a series of cross-linked AEMs using ring-opening metathesis polymerization of tetraalkylammonium-functionalized cyclic olefins [12,13]. Even though such methods are mature and widely used, unavoidable disadvantages remain. Primary is the excess use of toxic organic solvents as well as long preparation times and the need for intricate chemical processes. The resultant large quantities of waste present serious hazards and the risk of pollution to the environment. Therefore, there is a strong desire to develop a method of AEM preparation that does not involve any organic solvents.

In our previous work, a series of AEMs were prepared by a solvent free strategy aiming to solve the problems mentioned above [14]. The article highlight was the preparation of a special casting solution formed when cardo polyetherketone (PEK-C) and benzoyl peroxide (BPO) (polymer intensifier and initiator, respectively) were dissolved into a mixture of vinylbenzyl chloride (VBC) and divinylbenzene (DVB) monomers in the absence of additional organic solvents. After *in situ* polymerization and quaternization, the target AEMs were obtained, which involved an interpenetrating polymer network (IPN) structure composed of PEK-C and the copolymer of poly(VBC-co-DVB). Such method for AEM preparation presents environmental benefits and is worthy of further investigation. However, the chemical stabilities of AEMs were not fully qualified and the AEMs require improvement, in order to realize fuel cell application, due to the absence of microcosmic phase separation resulting from the lack of chemical interactions between the poly(VBC-co-DVB) and PEK-C components in the IPN structure. To this end, tetraethylenepentamine (TEPA), which would undergo facile reactions with the benzyl chloride groups of VBC and the phenolphthalein side groups of PKE-C (via nucleophilic substitution and lactamization reactions, respectively) was introduced in this study as a cross-linker. Considering the important role of the cross-linker, improved AEM chemical stabilities can be anticipated. Moreover, this innovation would not introduce the requirement for organic solvents so the environment benefits of the methodology will be preserved. Consequently, a series of cross-linked AEMs were prepared by dissolution of PEK-C and BPO into a mixture of VBC and DVB monomers followed by addition of TEPA and *in situ* polymerization and quaternization. The effect of TEPA and its apparent impact on AEM properties will be the focus of this study, while the casting solution formulation that was optimized in our previous work will be retained. In addition, initial beginning-of-life fuel cell performances will be measured in order to demonstrate that they have the potential to generate power in the end application.

2. Experiment

2.1. Materials

Cardo polyetherketone (PEK-C) (Mw = 115,000) was purchased from Xuzhou Engineering Plastic Factory (China), purified by reprecipitation from *N*,*N*-dimethylformamide (DMF) into deionized water and then dried at 50 °C. Vinylbenzyl chloride (VBC) was purchased from Changzhou Wujin Linchuan Chemical Co. Ltd. (China) and divinylbenzene (DVB) was purchased from Aldrich (Milwaukee, WI, USA); both of these monomers were purified by a treatment with aqueous NaOH solution (5%w/v). The thermal initiator benzoyl peroxide (BPO) and the cross-linker tetraethylenepentamine (TEPA) were purchased from China National Medicines Co. Ltd.; the former was recrystallized in chloroform and methanol and dried at 60 °C for 24 h before use.

2.2. Membrane preparation

Cross-linked AEMs were prepared similar to our previous work, whose optimized casting solution formulations were chosen for modification in this study [14]. As shown in Scheme 1, mixtures of 8 cm^3 VBC and 0.48 cm^3 DVB (6%) monomers were used to dissolve 2 g PEK-C (25%) and 0.48 g BPO (6%) (the DVB, PEK-C and BPO contents were calculated as their weight percentage with respect to VBC); controlled and varying amounts of TEPA were then added to these mixtures (see Table 1) in order to form the different AEMs. After ultrasonic treatment to remove the air bubbles, the final casting solutions were cast between two glass plates, which were then sealed with aluminum tape to avoid monomer volatilization. *In situ* bulk polymerizations were then carried out at 80 °C for 8 h; the resulting base membranes were finally immersed in an aqueous TMA solution (1 mol dm^{-3}) at 25 °C for quaternization and the formation of the target AEMs. To investigate the effect of TEPA on the performances of the base membranes, different base membranes with various TEPA content were prepared (Table 1). The TEPA content was calculated as a molar percentage with respect to PEK-C. The resultant base membranes were designated as PPT membranes (Poly(VBC-co-DVB) + PEK-C + TEPA) and the corresponding quaternized AEMs as QPPT membranes.

2.3. Membrane characterization

2.3.1. Morphological evaluation

The cross section morphologies of the membranes were examined using an environmental scanning electron microscope (ESEM) using a FESEM (Philips, FEI XL30).

2.3.2. Thermal analysis

TGA and DTG thermograms were recorded using a Shimadzu TGA-50H analyzer at heating rate of 10 °C min^{-1} under a N_2 atmosphere in order to evaluate the short-term thermal properties and stabilities of the AEMs.

2.3.3. Glass transition temperature (T_g) and tensile measurements

The glass transition temperature (T_g) was determined using a dynamic mechanical analyzer (TA instruments, DMAQ800). DMA studies were conducted over a temperature range of 25–250 °C, with a ramp rate of 5 °C min^{-1} in extension mode (sinusoidal stress of 10 Hz frequency). Tan δ (the ratio of the loss modulus to the storage modulus) was monitored as a function of temperature. The glass transition temperature (T_g) was taken to be the maximum in the loss-tangent versus temperature curve.

Tensile measurements were carried out using the same DMA analyser in controlled force mode using a stretch rate of 0.25 N min^{-1}.

2.3.4. Fourier transform infrared spectroscopy (FT-IR)

FT-IR spectra were measured using a Vector 22 Fourier transform infrared spectrometer (Bruker).

2.3.5. X-ray diffraction (XRD)

XRD was performed on a Japan Rigaku K/max-γA X-ray diffractometer with Cu Kα radiation (λ = 1.54,178 Å, 2θ = 0.5–2.8°) at the scanning rate of 0.02° s^{-1}.

2.3.6. Water uptake

Water uptakes were calculated by taking the difference between the wet weight (m_{wet}) and the dry weight (m_{dry}) of the AEMs. To

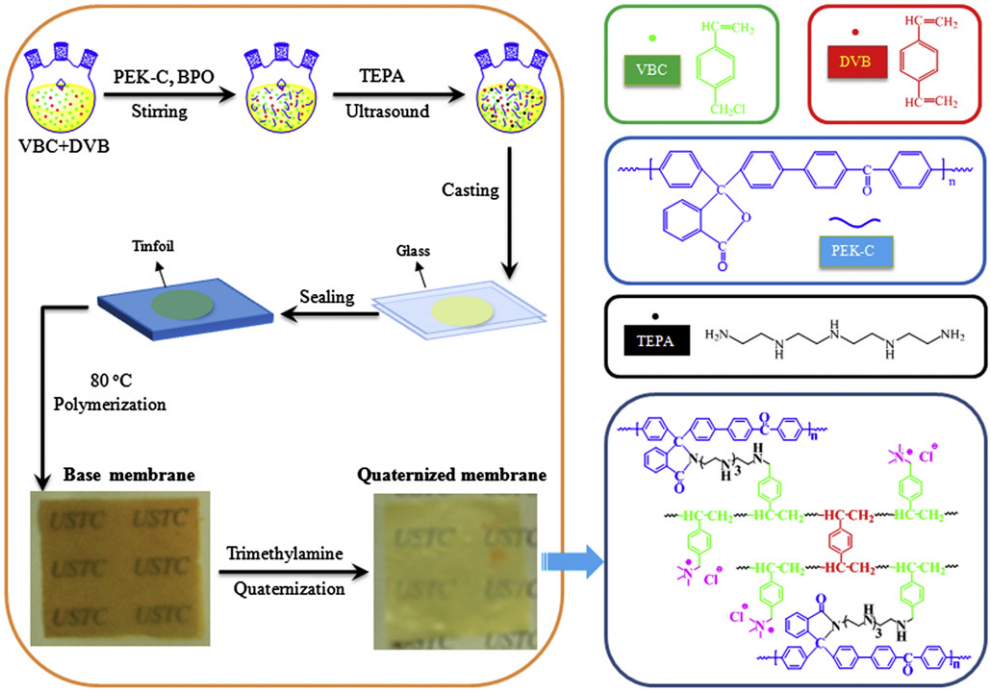

Scheme 1. Schematic of the solvent free strategy used to prepare the QPPT anion exchange membranes.

obtain the wet weight, AEM samples were equilibrated with distilled water at 25 °C for 2 days. The water uptakes were calculated according to the following equation:

$$W_R = \frac{m_{wet} - m_{dry}}{m_{dry}} \times 100\% \quad (1)$$

2.3.7. Ion exchange capacity

The ion exchange capacities (IEC) were measured according to our previous work [15]. The samples were firstly dried to a constant weight and then immersed in an aqueous Na_2SO_4 (0.5 mol dm^{-3}) solution for 2 days. The concentration of Cl^- released from the membrane was measured using a REX PHS-3C analyzer (China) and an attached Cl^- ion-selective electrode (model pCl-1). The IEC value was calculated from the measured amounts of released Cl^- ions and is expressed as mmol g^{-1} of the dry membrane.

2.3.8. Alkaline stability

The alkaline stabilities of the obtained AEMs were evaluated using the method reported in reference [16]: after immersion of the AEMs in an aqueous KOH (2 mol dm^{-3}) solution at 40 °C for different time periods, the residual IEC values were measured (as above). The IEC values before and after alkaline aging are denoted IEC_0 and IEC_t, respectively. The ratios of IEC_t to IEC_0 were used to determine the relative alkaline stabilities.

Table 1
The compositions of PPT base membranes produced in this study.

Sample	VBC g	DVB g	PEK-C g	BPO g	TEPA[a] (%)
PPT-5	8	0.48	2	0.48	5
PPT-10	8	0.48	2	0.48	10
PPT-15	8	0.48	2	0.48	15
PPT-20	8	0.48	2	0.48	20
PPT-25	8	0.48	2	0.48	25
PPT-30	8	0.48	2	0.48	30
PPT-35	8	0.48	2	0.48	35

[a] The TEPA content was calculated as a molar percentage with respect to PEK-C.

2.3.9. Ionic conductivity

The measurement of the AEMs' ionic conductivities, similar to that used for measurement of proton conductivities, involved the standard four-point probe technique [17]. Before measurement, the membrane samples were firstly immersed in an aqueous KOH (1 mol dm^{-3}) solution at room temperature for 24 h and then thoroughly washed by distilled water. The Teflon measuring cell contained two stainless steel flat outer current-carrying electrodes (2 cm separation) and two platinum wire inner potential-sensing electrodes (1 cm separation). A membrane sample in the hydroxide form (1 cm × 4 cm) was mounted in the cell and the resultant impedance was recorded using an Auto lab PGSTAT 302 (Eco Chemie, Netherlands) in galvanostatic mode with an a.c. current amplitude of 0.1 mA and a frequency range of 1 MHz–50 Hz. The ionic conductivity (σ) measurements were conducted at a variety of temperatures and relative humidities, which were controlled using an environmental chamber (LHS-100CL, Shanghai Yiheng Instrument, China). The ionic conductivity was calculated according to the following equation:

$$\sigma = \frac{L}{RWd} \quad (2)$$

where R is the membrane resistance, L is the distance between potential-sensing electrodes, and W and d are the width and thickness of the membrane, respectively.

2.3.10. Performance of an alkaline membrane fuel cell

Fuel cell testing was conducted according to previous reports [18,19].

2.3.10.1. Membrane electrode assembly. Catalyst inks were prepared by first mixing the Pt catalyst (HISPEC 3000: 20 wt% Pt/$Vulcan_{XC-72R}$, Johnson Matthey Plc., UK) and poly(vinylbenzyl chloride) with ethyl acetate solvent. After the mixture was sonicated for at least 30 min

in ultrasonic water-bath, the ink was carefully sprayed onto the top of a carbon microporous layer coating (20%mass PTFE binder, 1 mg_{carbon} cm^{-2}) located on one side of a wet-proofed carbon paper gas diffusion substrate (20%mass PTFE wet-proofing) until a Pt loading of 0.40 mg cm^{-2} was achieved. A poly(vinylbenzyl chloride) loading of 15%mass, with respect to the mass of Pt/C catalyst powder, was used. The dried catalyzed gas diffusion electrodes (identical anode and cathodes were used) were subsequently treated overnight with undiluted *N,N,N′,N′*-tetramethyl-1,6-hexanediamine (99%, Sigma–Aldrich). This yields Surrey's 1st generation ionomer (designated SION1) [20]. After washing with DI water, the electrodes were converted to OH^- as for the QPPT membrane synthesis. The alkaline AEM (AAEM) QPPT-35 was then sandwiched between the two electrodes, with catalyst layer facing the AAEM, and the resultant MEA was assembled into the fuel cell fixture without pre-assembly hot-pressing.

2.3.10.2. Fuel cell testing. The performances of MEA (electrode geometric area of 5.3 cm^2) were measured in a Scribner 850e fuel cell test station (Scribner Associates Inc., USA) without gas back pressurization. The test cell composes of a pair of graphite bipolar plates, machined with serpentine flow fields, two gold-coated current collector plates and two stainless steel end plates for holding the bipolar plates firmly in place. Rod heaters were inserted into the end plates to control the cell temperature. The prepared MEAs were correspondingly sandwiched in between two gaskets (thickness = 0.15 mm) and sealed into the test cell at a constant torque of 5.5 N m, using retaining bolts and a torque wrench. Fuel Cell® software version 4 (Scribner Associates) was used to record the galvanostatic polarization curves of the fuel cell. The input flow rates of anode hydrogen and cathode oxygen (both industrial grade, BOC) were respectively controlled at 600 cm^3 min^{-1}. The humidification temperatures of anode and cathode were controlled at the cell temperature of 50 °C, achieving the calculated relative humidity (RH) = 100%. Prior to polarization curve measurement, the assembled cells were activated by operation of the cell at open circuit voltage (OCV) for 1 h, followed by potentiostatic discharge control at 0.1 V and then 0.5 V for 30 min each (or until a stable constant current was obtained).

3. Result and discussion

3.1. Preliminary experiments

As mentioned above, TEPA was used as the cross-linker to improve the chemical stabilities of AEMs, which were based on the optimized casting solution formulations from our previous work [14]. In preliminary experiments, we found that the viscosity of the casting solutions increased greatly on addition of TEPA due to its rapid reactions with VBC and TEPA; this required the use of more BPO to ensure the fully polymerization because of the highly decreased polymerization efficiency as reported previously [14]. Therefore, there is a need to investigate the film forming properties of the base membranes with various combinations of TEPA and BPO contents. It is obvious from the data in Table 2 that the content of TEPA must be <40% to avoid undesirable precipitation and the content of BPO should be >6% to guarantee full polymerization. For simplicity, the BPO content, with PPT membranes containing TEPA contents of 5–35%, was finally fixed at 6% for the next step research.

Scheme 1 shows the photographs of the PPT base membrane and the QPPT quaternized membrane (taken using Canon EOS 7D digital SLR camera). As can be seen, PPT membrane is dark yellow while QPPT membrane is paler in color. Both membranes are uniform in macroscopic appearance, semitransparent and flexible and they can easily be cut to the desired size.

Table 2
Qualitative assessment of the film forming properties of the PPT base membranes as a function of TEPA and BPO contents.

Group	VBC g	DVB g	PEK-C g	TEPA (%)	BPO (%)			
					2	4	6	8
1#	8	0.48	2	5	√	√	√	√
2#	8	0.48	2	15	√	√	√	√
3#	8	0.48	2	30	×	√	√	√
4#	8	0.48	2	35	×	×	√	√
5#	8	0.48	2	40	–	–	–	–

×: poor/unmeasurable; √: good; –: precipitate formed.

3.2. FT-IR

FT-IR analysis was utilized to confirm the structure of PPT membranes (Fig. 1). For poly(VBC-co-DVB), the bands at 2950 and 2850 cm^{-1} are attributed to $-CH_2$ and $-CH$ stretching vibration whereas the band at 680 cm^{-1} is attributed to C–Cl stretching vibration [21]. For PEK-C, its characteristic absorption band was observed at 1770 cm^{-1} due to C=O (–COO– in cardo group) stretching vibration [22]. Moreover, both of their characteristic bands as mentioned above are all observed in PPT membranes, indicating the successful blend of poly(VBC-co-DVB) and PEK-C in PPT membranes.

3.3. SEM and XRD

In order to investigate the effect of TEPA on the morphologies of the PPT membranes, the cross sections of PPT-5–PPT-20 were studied using SEM (Fig. 2). For the lower TEPA content membranes, PPT-5 and PPT-10, smooth cross sections with a uniform distribution of PEK-C and poly(VBC-co-DVB) (Fig. 2(a) and (b)) are observed; the poly(VBC-co-DVB) component is dispersed as spherical domains in a continuous PEK-C matrix with clearly demarcated boundaries. This phenomenon was also observed in our previous work and was explained by a space volume contraction during the free radical polymerization of VBC and DVB [14]. In comparison, PPT-15 (Fig. 2(c)) shows a different morphology even though a uniform distribution of PEK-C and poly(VBC-co-DVB) is retained. Its cross section becomes rugged and the boundaries between poly(VBC-co-DVB) and PEK-C components are more

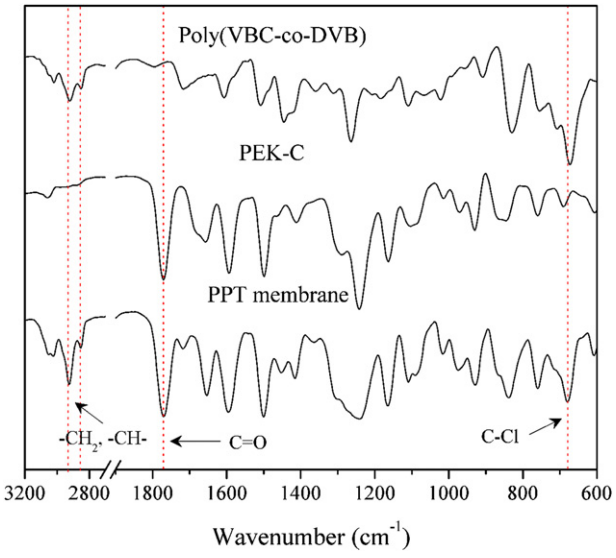

Fig. 1. FT-IR spectra of poly(VBC-co-DVB), PEK-C and PPT membrane.

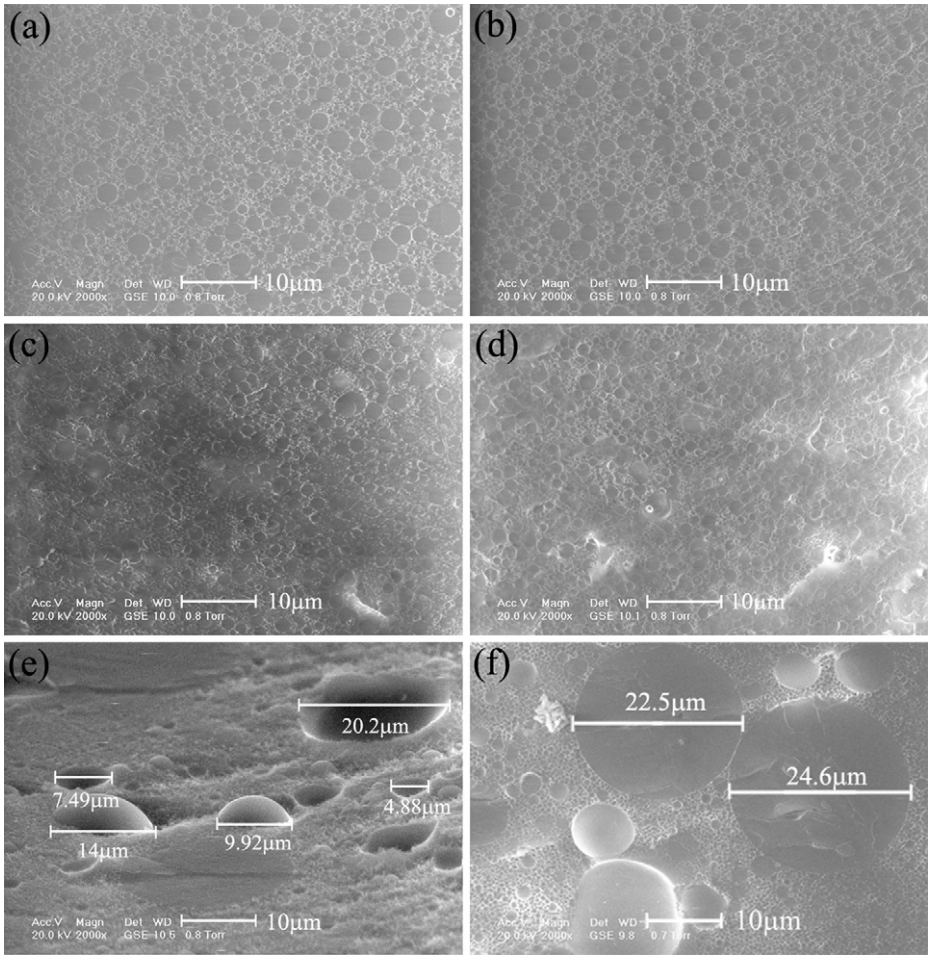

Fig. 2. SEM micrographs of the cross sections of the base PPT membranes with increasing TEPA content: (a) PPT-5 (5%TEPA + 6%BPO), (b) PPT-10 (10%TEPA + 6%BPO), (c) PPT-15 (15%TEPA + 6%BPO) and (d) PPT-20 (20%TEPA + 6%BPO). Also included are SEM micrographs of our previous reported membranes [14] produced using the same solvent-free methodology but without addition of TEPA: (e) 3%BPO and (f) 4%BPO.

obscure and often accompanied by the appearance of a white ring. Such phenomenon is explained by the cross-linking effect of TEPA. For PPT-5 and PPT-10, the degree of cross-linking is relatively lower, consequently affording two phases with relatively weaker intermolecular interactions and the resulting well defined boundaries. With a further increase in TEPA content (PPT-15), the interactions will be stronger resulting in higher compatibility between the two main phases and the obscuring of the boundaries. This result highlights the positive effect of TEPA on the morphologies of the PPT membranes with respect to the enhanced compatibility between the poly(VBC-co-DVB) and PEK-C components. The white rings observed at the boundaries may be a new phase between PEK-C and poly(VBC-co-DVB); this will be discussed in the next section that describes the glass transport temperature (T_g) measurements. For PPT-20 (Fig. 2(d)), there is no significant difference compared to PPT-15 with a decreased level of definition of the boundaries and an increased width of the white rings (resulting from further increases in the intermolecular interactions and cross-linking degree between the two phases).

In our previous work, it was observed that the base membranes synthesized without the addition of TEPA would suffer serious (undesirable) phase separations when the BPO content was >3% due to an auto-acceleration effect resulting from the high viscosity [14]. As can be seen in Fig. 2(e) and (f), numerous discrete poly(VBC-co-DVB) particle with diameters 7.5–24.5 μm are observed

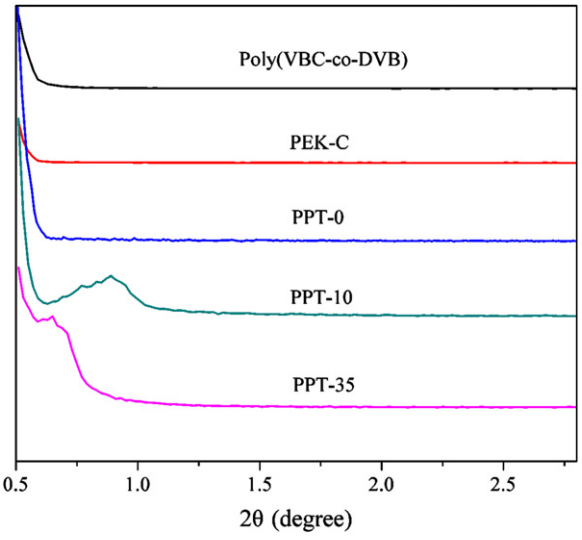

Fig. 3. XRD profiles including small angle region of poly(VBC-co-DVB), PEK-C, PPT-10 and PPT-35.

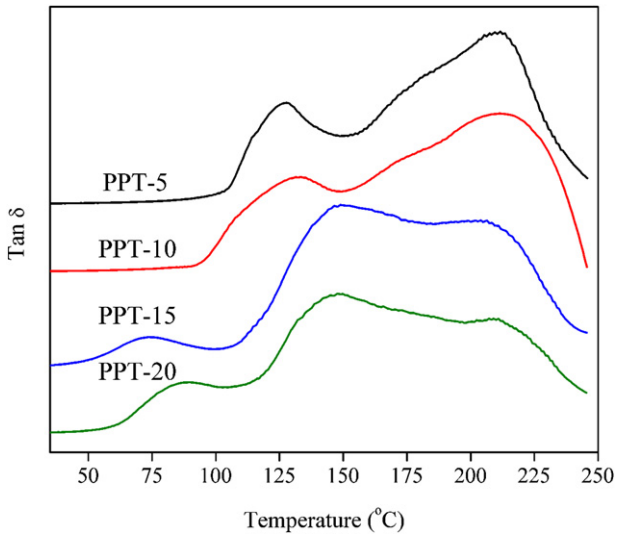

Fig. 4. Tan δ versus temperature DMA curves of the PPT membranes.

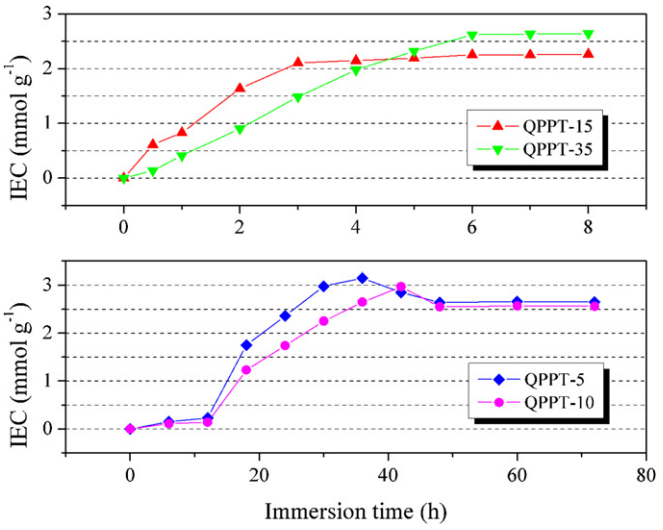

Fig. 5. The IEC values of select QPPT membranes as a function of PPT immersion time. Quaternization was performed in an aqueous TMA solution (1 mol dm^{-3}) at 25 °C.

in the cross sections of the base membranes reported previously [14] (that do not contain TEPA). In contrast, this segregation phenomenon is not observed for the PPT membranes containing TEPA (Fig. 2(a–d)) even with BPO contents as high as 6%. This is an important result and demonstrates that TEPA significantly inhibits the auto-acceleration effect during polymerization and consequently improves the compatibility of PEK-C and poly(VBC-co-DVB) components.

XRD including small angle region (2θ = 0.5–2.8°) were also presented and poly(VBC-co-DVB), PEK-C, PPT-0 (without the addition of TEPA), PPT-10 and PPT-35 were chosen for the investigation (Fig. 3). No obvious peak was observed in both of poly(VBC-co-DVB) and PEK-C profiles, it is easy to be understood as both of them are amorphous polymer the phenomenon is similar to that of PPT-0. In contrast, the crystal cell (2θ = 0.88°) in PPT-10 can be attributed to the formation of the partial ordered microphase structure [23]. The new observations along with addition of TEPA indicates the cross-linking effect of TEPA furthermore [23], in addition, the long period (*ca.* 100 Å) may imply that the components are trapped between and dispersed in a common lamellar [24–26]. This may be due to the effect of TEPA as cross-linker, which enhances the interaction force between the blending components in membrane. For PPT-35 with a increasing TEPA content, the long period increases to *ca.* 130 Å, signifying the increased amount of components being trapped [25] and may be due to the further enhanced interaction force between components resulting from TEPA. These results are consistent with SEM observation to a certain degree.

3.4. Glass transition temperature (T_g) measurement

The glass transition temperatures (T_g) of the PPT membranes were measured to further investigate the compatibility between the poly(VBC-co-DVB) and PEK-C. It is well known that the difference in T_g (ΔT_g) between the two phases is a direct determination of their compatibility [27]. Using the SEM observations above, PPT-5 to PPT-20 were selected for DMA analyses, where the T_gs of the PPT membranes were measured from tan δ peak versus temperature curves (Fig. 4); the resulting data is summarized in Table 3. As expected, the T_g values depend on the TEPA content. Specifically, PPT-5 with lowest TEPA content, possesses two T_g values, the first one (T_{g1}) at *ca.* 120 °C is attributed to the poly(VBC-co-DVB) phase while the second one (T_{g3}) at *ca.* 212 °C is attributed to the PEK-C phase [28]; this is also observed for PPT-10. In contrast, three T_g values were observed for PPT-15 produced using a higher TEPA content; the new T_{g3} at *ca.* 74 °C is attributed to a new phase, which is relatively more flexible as indicated by the lower T_g value. As discussed above, white rings were observed at the boundaries between PEK-C and poly(VBC-co-DVB) phases in the SEM cross sections of PPT-15, resulting from the cross-linking effect of TEPA. When considering the flexible aliphatic chain of TEPA, the appearance of T_{g3} in PPT-15 is attributed to a flexible cross-linking phase between PEK-C and poly(VBC-co-DVB) (the white rings). Besides, the $\Delta(T_{g2} - T_{g1})$ value for PPT-15 (*ca.* 60 °C) is lower compared to PPT-5 (*ca.* 85 °C) and PPT-10 (*ca.* 82 °C), which

Table 3
Glass transition temperatures, T_g, of the PPT base membranes measured from tan δ peak versus temperature DMA curves.

Samples	T_{g1} (°C)	T_{g2} (°C)	T_{g3} (°C)	$\Delta(T_{g2} - T_{g1})$ (°C)
PPT-5	127	212	–	85
PPT-10	131	213	–	82
PPT-15	148	208	74	60
PPT-20	150	207	89	57

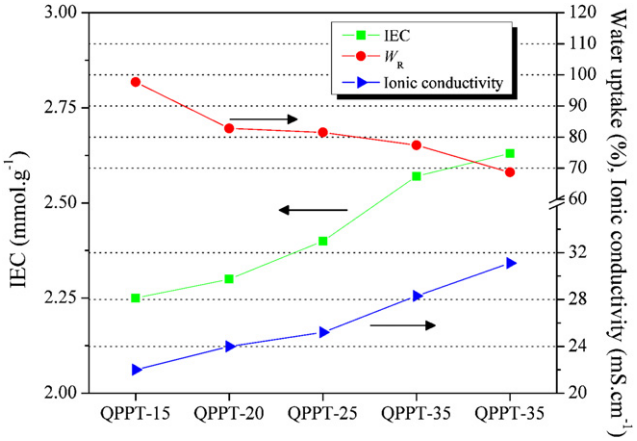

Fig. 6. The IEC, W_R and ionic conductivities of the QPPT membranes made using quaternization with an aqueous TMA solution (1 mol dm^{-3}) at 25 °C for 8 h.

represents additional evidence of significantly improved compatibility between the PEK-C and poly(VBC-co-DVB) phases. These results are fully consistent with the SEM observations detailed above. PPT-20 presents a similar result to that of PPT-15 but with a higher T_{g3} of 89 °C for PPT-20 (compared to 74 °C for PPT-15); this indicates the hardening of the cross-linking phase resulting from a decrease in free volume due to the enhanced degree of cross-linking degree in PPT-20.

3.5. Quaternization process

For application in APEFCs the anion-exchange forms are required so the PPT base membranes were immersed in an aqueous trimethylamine (TMA, 1 mol dm^{-3}) solution at 25 °C to introduce quaternary ammonium (QA) groups and yield the desired QPPT AEMs. Obviously, the density of QA groups is an important parameter due to its effect on water uptake and ionic conductivity. As the other conditions are fixed, the immersion time of the PPT membranes in the TMA solution is worthy of investigation. Specifically, PPT-5, 10, 15, and 35 were chosen for this quaternization investigation and the resulting ion exchange capacities (IEC) of the resulting QPPT membranes as a function of immersion time are presented in Fig. 5.

With increasing immersion time, the IECs of QPPT-5 and QPPT-10 first increase, and then plateau after *ca.* 48 h, while those of QPPT-15 and QPPT-35 plateau after *ca.* 6 h. This can be explained by the compactness of the PPT membranes as related to the morphologies shown in Fig. 1. When the TEPA content was <10%, both PPT-5 and PPT-10 displayed smooth cross sections with a dense structure. In contrast, when the TEPA content was >15%, the PPT cross sections were more rugged with a looser structure. The compactness of the PPT membranes would affect the reactions with TMA and consequently the final IECs obtained.

It was observed that both QPPT-5 and QPPT-10 were fragile, easily broken and showed seriously undesirable rough and wrinkled surfaces; these traits result from excessively swelling due to the lower cross-linking degree. In contrast, QPPT-15 and QPPT-35 were mechanically stable, flexible and showed a macroscopically uniform surface. Therefore, TEPA levels need to be >15% to ensure non-excessive swelling stabilities and maintained mechanical strength in the resultant QPPT membranes. For the next investigative stage detailed below (looking at key QPPT properties such as IEC), the TMA immersion time, with PPT membranes containing TEPA contents of 15–35%, was fixed at 8 h.

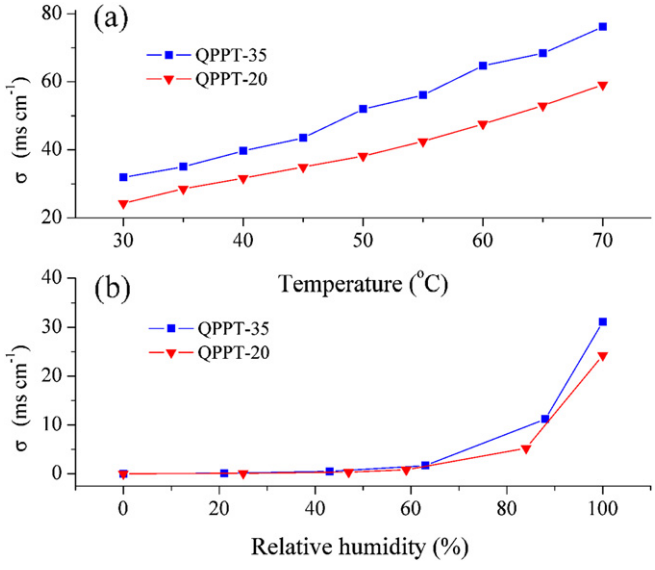

Fig. 7. The humidity dependence and temperature dependence of the ionic conductivity of the QPPT-20 and QPPT-35 membranes. (a) Conductivity as a function of temperature at 100% relative humidity, (b) Conductivity as a function of relative humidity at 30 °C.

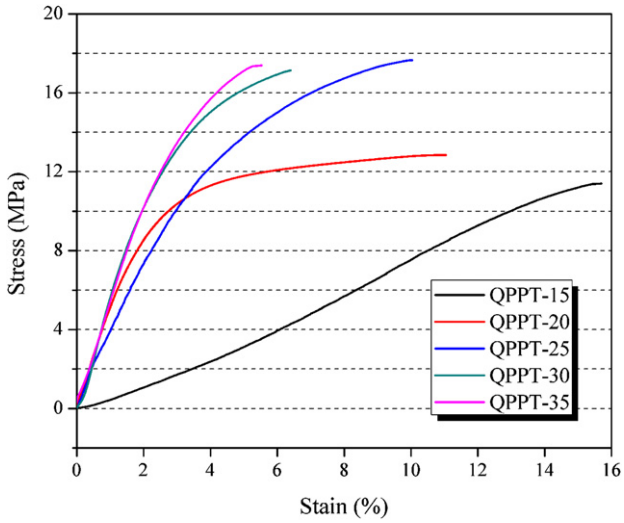

Fig. 8. Stress strain curves of QPPT AAEMs.

3.6. IEC and W_R, and ionic conductivity

After quaternization, the ion exchange capacity (IEC), water uptake (W_R) and ionic conductivities (σ) of the QPPT membranes were measured (Fig. 6). With increasing TEPA contents (from QPPT-15 to QPPT-35) the resulting IECs steadily increase from 2.30 to 2.63 mmol g^{-1}. Without cross-linking, W_R would be expected to increase with the increases in IEC due to water adsorption associated with the increase in the number of hydrophilic ion exchange groups. However, the results reveal that the W_R values decrease from 98% to 69% (from QPPT-15 to QPPT-3). This phenomenon is easily explained by the enhanced degree of cross-linking leading to a decrease in the free-volume in the membrane matrix for water adsorption. For the application of AEMs in APEFCs, ionic conductivity is a critical parameter. The ionic conductivities of the QPPT AAEMs increase from 22 to 31 mS cm^{-1} (QPPT-15–QPPT-35). Considering the increase in IEC, the result is easy to be

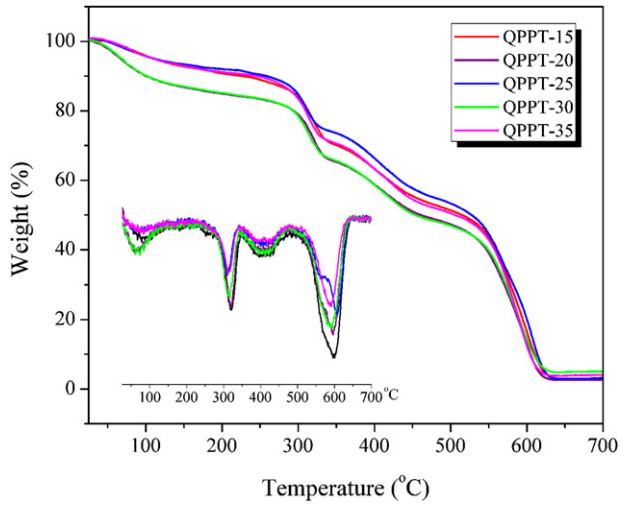

Fig. 9. TGA and DTG (inset) traces for the QPPT membranes recorded with a heating rate of 10 °C min^{-1} and under an N_2 flow.

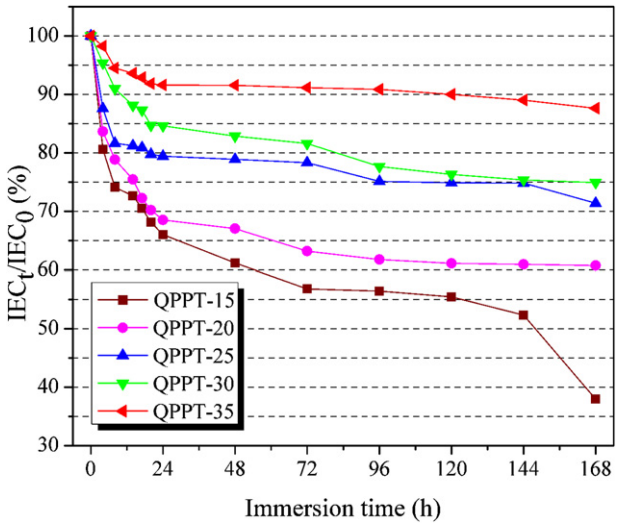

Fig. 10. A plot of the change in the IECs of the QPPT membranes after the immersion in an aqueous KOH (2 mol dm^{-3}) solution at 40 °C. IEC$_t$ = the IEC at time = t (in h) aging time, and IEC$_0$ = the IEC of the unaged membranes.

understood; further considering the downward trend in W_R (the presence of water is considered to facilitate the ionic conduction in ion exchange membranes), the result herein is especially good. For comparison, the optimized AEMs without TEPA reported in our previous work gave IECs = 1.43–1.76 mmol g^{-1}, W_R = 53–58%, and ionic conductivities = 19–22 mS cm^{-1} [14]. All parameters were much lower than the corresponding ones in this study, again highlighting the positive effect of the addition of TEPA.

As the relatively important parameter, ionic conductivity of QPPT membranes at a variety of temperatures and relative humidities were measured (Fig. 7). The chosen QPPT-20 and QPPT-35 all show a growing trend with the increase in either temperature or humidity. The former is due to the enhanced flexibility of polymer main chain [29] and the faster diffusion and thermal motion of hydroxide ions [30] while the latter was due to the easier dissociation by the water adsorbed [31]. It is worth noting that QPPT-35 presents an ionic conductivity of 76 mS cm^{-1} at 70 °C and 100% relative humidity, which is in favor of its application in AFC.

3.7. Mechanical property

The mechanical properties of the QPPT membranes were evaluated using tensile stress–strain measurements (Fig. 8). From QPPT-15 to QPPT-35, the tensile strength initially increases from 11 MPa to 17 MPa and then stabilizes at this level, while the strain behavior (elongation at break) shows an ever decreasing trend from 16% to 6%. These trends are again clearly attributed to the effect of TEPA; additional cross-linking enhances the tensile strength and simultaneously retards QPPT deformation. These values compare favorably to the cross-linked AEMs reported by Coates et al., which exhibit 7.2% strain at 16 MPa [12].

3.8. Thermogravimetric analysis (TGA)

The short-term thermal stabilities of the QPPT membranes were measured using TGA analysis (Fig. 9). As can be seen, the results from the different QPPT membranes are similar. The slight mass loss observed at temperatures <120 °C is due to the evaporation of absorbed water by the hydrophilic QA groups. Therefore, there is no obvious polymer-derived mass loss below temperatures of 250 °C, indicating the excellent short-term thermal stabilities of the QPPT membranes. The derivative curve (DTG, the inset in Fig. 6) can be used to differentiate between the different stages of thermal decomposition. For the three polymer-derived degradation peaks in the DTG plots, the mass loss in the range 250–350 °C is related to the decomposition of QA groups [32], which is higher than that of our previous work (200–300 °C) on the non-TEPA analogs [14]. The mass loss in the range 400–480 °C is due to the decomposition of the carbon containing chain, while the last (more severe) mass loss in the range 500–600 °C derives from the decomposition of phenyl groups [33].

3.9. Medium-term alkaline stability

The long term stability of AAEMs to alkali, for use in APEFCs, is a critically important parameter (considering the alkaline operating environment of APEFCs). To investigate the alkaline stabilities of the QPPT AEMs, they were immersed in an aqueous KOH (2 mol dm^{-3}) solution at 40 °C for 168 h; the ratios of IEC$_t$ (alkaline treated) to IEC$_0$ (untreated) were recorded at the increasing alkali aging time (Fig. 10), as reported previously [16]. The same trend is observed for all QPPT membranes where the IEC ratios show an initial rapid decrease in IEC with aging time followed by a region of stabilization at longer aging times. The loss in IEC is due to the well known degradation of QA groups via the direct nucleophilic substitution of the OH^- anion at the α-carbons [34–36]. Of more scientific interest in the apparent increase in stability with an increase in TEPA content. Specifically, the residual IEC for aged QPPT-15 after 168 h is *ca.* 40% but is *ca.* 60% for QPPT-20 (a significant 20% point increase). With a further increase in TEPA content to 35% (QPPT35), the residual IEC is nearly 90% after 168 h. In our previous work on non TEPA-analog AEMs, the alkaline stabilities were poor due to the lack of interaction forces between the PEK-C and poly(VBC-co-DVB) components; only 60% of the original IEC remained after 96 h aging in aqueous KOH (2 mol dm^{-3}) solution at a lower temperature of 25 °C [14]. The stability benefit of the additional cross-linking is self evident over the time scales investigated.

Table 4
Comparison of the key properties of the optimized AEM produced in this study to select literature reported AEMs.

Membranes	QPPT-35	Optimized QPP AEMs[a] [14]	Hybrid AEMs in Ref. [28]	BPPO based AEMs in Ref. [29]
Preparation process	*In situ* bulk polymerization	*In situ* bulk polymerization	Polymerization of VBC in toluene	BPPO modification in chlorobenzene
Solvent disposal	–	–	Evaporation into air	Evaporation into air
IEC (mmol g^{-1})	2.63	1.43–1.76	1.70–2.20	1.27–2.05
Water uptake (%)	68.7	57.9–82.5	16.3–35.0	45.2–325.9
Ionic conductivity (mS cm^{-1})	31	19–22	0.23–0.43	1–8.5
Duration in 2 mol L^{-1} KOH/NaOH solution	88% IEC remained after 168 h at 40 °C	60% IEC remained after 96 h at 25 °C	–	60% IEC remained after 192 h at 25 °C
Mechanical properties	Flexible and strong	Elastic and strong	Brittle	Brittle and strong
Thickness (μm)	140	60–80	65–103	85–110

[a] Our previously reported AEM prepared using a similar solvent-free method but without the addition of TEPA.

3.10. Brief comparison with the prior literature

Considering the application relevant properties such as IEC, W_R, ionic conductivity and alkaline stability, QPPT-35 appears the most optimized AEM in this study. It was chosen for comparison with select other prior reported AEMs (summarized in Table 4). For two prior AEMs prepared from polymerization of VBC in toluene [37] and modification of bromomethylated poly(2,6-dimethyl-1,4-phenylene oxide) (BPPO) in chlorobenzene [38], a large number of toxic organic solvents were used during their preparation, and their preparations involved long preparation times and complex procedures; moreover, the large quantities of waste were directly emitted into the air by solvent evaporation. In contrast, the methodology used in this study should dictate the absence of organic solvents, and therefore reduce the subsequent waste (highlighting the excellent environmental and economic advantage of the methodology adopted). The QPPT-35 AEM also possesses higher IEC, higher ionic conductivity and improved alkaline stability. For the optimized non-TEPA AEMs reported in our previous work, the main drawback was relatively poor alkaline stability (as detailed above) [14]. In contrast, the addition of TEPA significantly improved the medium-term alkaline stability of QPPT-35 as well as yielding improvements in fuel cell related parameters such as ionic conductivity. Generally, QPPT-35 shows high IEC, good alkaline resistance, favorable mechanical properties and high ionic conductivity, which are comparable to or higher than those of the referenced AEMs [37,38]; this all indicates that QPPT-35 can be evaluated in a fuel cell.

3.11. Fuel cell performance

Given the properties of QPPT-35 detailed above, it was chosen as an exemplar for evaluation in a simple single cell fuel cell. Fig. 11 shows the fuel cell performance data of QPPT-35, where the open circuit voltage (OCV) of the single cell is 1.08 V and a peak power density of 6 mW cm^{-2} (geometric) is obtained at a current density of 11 mA cm^{-2}. Compared with our previous quaternary guanidinium AAEMs, which exhibited a power density of 16 mW cm^{-2} [39] when tested under the same test conditions, on the same test equipment, and with the same non-optimal ionomer, the result herein is acceptable and indicates the potential of the solvent free AEMs for application for APEFCCs. Simultaneously, the changes in current density at 0.2 V voltage were measured for extended periods during the H_2/O_2 fuel cell operation to investigate the cell stability (Fig. 12). Unfortunately, the current density cannot remain

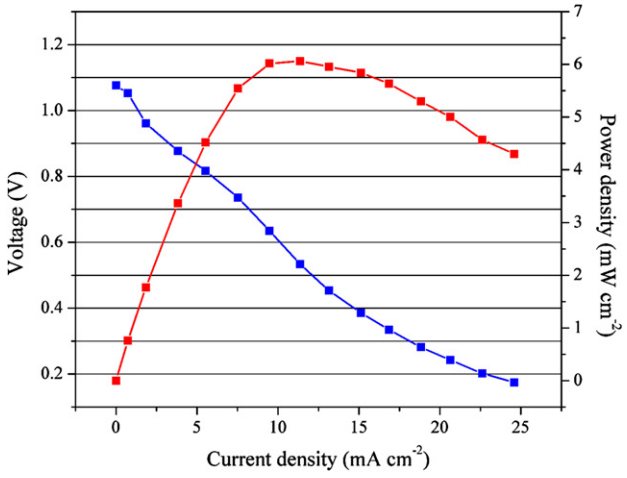

Fig. 11. Beginning-of-life H_2/O_2 fuel cell performance curves at 50 °C containing the QPPT-35 AAEM.

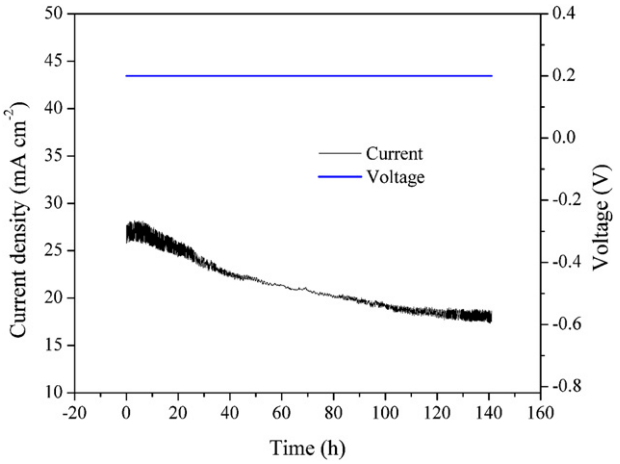

Fig. 12. The changes in current density at 0.2 V during the H_2/O_2 fuel cell operation.

stable and *ca*. 30% loss is observed after 140 min. However, QPPT AEMs herein are still worth to be optimized as considering the environmental benefits of the preparation method. Moreover, the development of thinner AEMs and also of a chemically related and dispersible form (for use as the alkaline ionomer [anionomer] in the catalyst layers of the membrane electrode assemblies) is now desired to truly assess the performance capabilities of this class of anion-exchange polymer electrolyte in operating fuel cells.

4. Conclusions

Cross-linked AEMs (being developed for application in alkaline polymer electrolyte fuel cells) were successfully prepared using an environmentally friendly solvent free strategy. The monomer mixture (vinylbenzyl chloride [VBC] and divinylbenzene [DVB]) was used to dissolve the cardo-polyetherketone (PEK-C) base polymer instead of organic solvents. Tetraethylenepentamine (TEPA) was added to the casting solution as a cross-linker as it reacts rapidly with benzyl chloride groups, such as those of VBC, and the phenolphthalein side group of PEK-C by nucleophilic substitution and lactamization reactions respectively. *In situ* polymerization and quaternization were then conducted yielding the target cross-linked AEMs. The effect of TEPA on the performance of the pre-quaternized intermediate membranes was fully investigated. The results showed that TEPA not only improves the compatibility between the poly(VBC-co-DVB) and PEK-C components but also enhances the membrane performance, especially the medium-term stability to alkali. Moreover, a single H_2/O_2 fuel cell test, on the best performing AEM example, yielded a power density of 6 mW cm^{-2}, which shows that this class of membrane can produce reasonable *in situ* performances even when fabricated in non-optimized membrane–electrode assemblies. The reported AEMs show promise for potential application in solid alkaline fuel cells but further optimizing is still needed especially the stability during the cell operation.

Acknowledgments

We thank the financial supports from the National Natural Science Foundation of China (nos. 21106140, 21025626 and J1030412), the National Basic Research Program of China (No. 2012CB932800), National High Technology Research and Development Program 863 (2012AA03A608), and the Programs of Anhui Province for Science and Technology (No. 11010202157). The University of Surrey researchers were supported by the UK's Engineering and Physical Sciences Research Council (grants EP/I004882/1 and EP/H025340/1).

References

[1] G. Merle, M. Wessling, K. Nijmeijer, Journal of Membrane Science 377 (2011) 1–35.
[2] J.R. Varcoe, R.C.T. Slade, Fuel Cells 5 (2005) 187–200.
[3] Y. Wang, K.S. Chen, J. Mishler, S.C. Cho, X.C. Adroher, Applied Energy 88 (2011) 981–1007.
[4] G. Couture, A. Alaaeddine, F. Boschet, B. Ameduri, Progress in Polymer Science 36 (2011) 1521–1557.
[5] J.R. Varcoe, R.C.T. Slade, G.L. Wright, Y. Chen, The Journal of Physical Chemistry B 110 (2006) 21041–21049.
[6] M.A. Al-Saleh, S. Gultekin, A.S. Al-Zakri, H. Celiker, International Journal of Hydrogen Energy 19 (1994) 713–718.
[7] F. Pagnanelli, C. Sambenedetto, G. Furlani, F. Vegliò, L. Toro, Journal of Power Sources 166 (2007) 567–577.
[8] J. Fang, P.K. Shen, Journal of Membrane Science 285 (2006) 317–322.
[9] G. Wang, Y. Weng, D. Chu, R. Chen, D. Xie, Journal of Membrane Science 332 (2009) 63–68.
[10] Y. Xiong, Q.L. Liu, Q.H. Zeng, Journal of Power Sources 193 (2009) 541–546.
[11] Y. Luo, J. Guo, C. Wang, D. Chu, Electrochemistry Communications 16 (2012) 65–68.
[12] T.J. Clark, N.J. Robertson, H.A. Kostalik IV, E.B. Lobkovsky, P.F. Mutolo, H.C.D. Abruña, G.W. Coates, Journal of the American Chemical Society 131 (2009) 12888–12889.
[13] N.J. Robertson, H.A. Kostalik, T.J. Clark, P.F. Mutolo, H.C.D. Abruña, G.W. Coates, Journal of American Chemical Society 132 (2010) 3400–3404.
[14] X. Lin, M. Gong, Y. Liu, L. Wu, Y. Li, X. Liang, Q. Li, T. Xu, Journal of Membrane Science 425–426 (2013) 190–199.
[15] X. Tongwen, Y. Weihua, Journal of Membrane Science 190 (2001) 159–166.
[16] E.N. Komkova, D.F. Stamatialis, H. Strathmann, M. Wessling, Journal of Membrane Science 244 (2004) 25–34.
[17] Y. Sone, P. Ekdunge, D. Simonsson, Journal of The Electrochemical Society 143 (1996) 1254–1259.
[18] J.R. Varcoe, R.C.T. Slade, Electrochemistry Communications 8 (2006) 839–843.
[19] J.R. Varcoe, R.C.T. Slade, E.L.H. Yee, S.D. Poynton, D.J. Driscoll, Journal of Power Sources 173 (2007) 194–199.
[20] R. Zeng, S.D. Poynton, J.P. Kizewski, R.C.T. Slade, J.R. Varcoe, Electrochemistry Communications 12 (2010) 823–825.
[21] X. Hankun, F. Jun, G. Mingli, L. Xiaohuan, W. Xiaolan, T. Song, Journal of Membrane Science 354 (2010) 206–211.
[22] L.C. Li, B.G. Wang, H.M. Tan, T.L. Chen, J.P. Xu, Journal of Membrane Science 269 (2006) 84–93.
[23] A.J. Ryan, W.R. Willkomm, T.B. Bergstrom, C.W. Macosko, J.T. Koberstein, C.C. Yu, T.P. Russell, Macromolecules 24 (1991) 2883–2889.
[24] G.D. Wignall, J.D. Londono, J.S. Lin, R.G. Alamo, M.J. Galante, L. Mandelkern, Macromolecules 28 (1995) 3156–3167.
[25] H. Abe, Y. Doi, M.M. Satkowski, I. Noda, Macromolecules 27 (1994) 50–54.
[26] C.H. Lee, T. Okada, H. Saito, T. Inoue, Polymer 38 (1997) 31–34.
[27] P.R. Couchman, Macromolecules 11 (1978) 1156–1161.
[28] W. Liu, T. Chen, J. Xu, Journal of Membrane Science 53 (1990) 203–213.
[29] B. Lin, L. Qiu, J. Lu, F. Yan, Chemistry of Materials 22 (2010) 6718–6725.
[30] D.S. Kim, G.P. Robertson, M.D. Guiver, Macromolecules 41 (2008) 2126–2134.
[31] K. Ogura, T. Saino, M. Nakayama, H. Shiigi, Journal of Materials Chemistry 7 (1997) 2363–2366.
[32] J. Wang, Z. Zhao, F. Gong, S. Li, S. Zhang, Macromolecules 42 (2009) 8711–8717.
[33] L.A. Wu, G.F. Zhou, X. Liu, Z.H. Zhang, C.R. Li, T.W. Xu, Journal of Membrane Science 371 (2011) 155–162.
[34] J.A. Vega, C. Chartier, W.E. Mustain, Journal of Power Sources 195 (2010) 7176–7180.
[35] T. Sata, M. Tsujimoto, T. Yamaguchi, K. Matsusaki, Journal of Membrane Science 112 (1996) 161–170.
[36] Q. Zhang, Q. Zhang, J. Wang, S. Zhang, S. Li, Polymer 51 (2010) 5407–5416.
[37] Y. Wu, C. Wu, T. Xu, F. Yu, Y. Fu, Journal of Membrane Science 321 (2008) 299–308.
[38] Y. Wu, C. Wu, T. Xu, X. Lin, Y. Fu, Journal of Membrane Science 338 (2009) 51–60.
[39] X. Lin, L. Wu, Y. Liu, A.L. Ong, S.D. Poynton, J.R. Varcoe, T. Xu, Journal of Power Sources 217 (2012) 373–380.